BBA - Biomembranes 1864 (2022) 183911

Contents lists available at ScienceDirect

BBA - Biomembranes

journal homepage: www.elsevier.com/locate/bbamem

# WIND-PVPA: Water/Ion NMR Detected PVPA to assess lipid barrier integrity *in vitro* through quantification of passive water- and ion transport

Philip Rainsford [a,1], B. Ravdna Sarre [a,1], Margherita Falavigna [b], Bjørn Olav Brandsdal [a], Gøril Eide Flaten [b], Martin Jakubec [a,1], Johan Isaksson [a,*,1]

[a] Dept. Chemisty, UiT the Arctic University of Norway, 9037 Tromsø, Norway
[b] Dept. Pharmacy, UiT the Arctic University of Norway, 9037 Tromsø, Norway

ARTICLE INFO

*Keywords:*
Nuclear magnetic resonance
PVPA
Permeability assay
Water permeability
Salt permeability
Antimicrobial peptides
Lipid vesicles

ABSTRACT

Water/Ion NMR Detected – Phospholipid Vesicle Permeability Assay (WIND-PVPA), is presented as a novel, straightforward and automatable method to assess lipid barrier integrity *in vitro*. The apparent permeability constants of water- and ions across the PVPA barriers are determined in a one-pot experiment under the influence of membrane-active guest molecules. NMR spectroscopy is used to quantify the water directly ($D_2O$) and the ions indirectly (complexed with EDTA) as a function of time. WIND-PVPA is demonstrated using four anti-microbial peptides, to show that membrane active molecules can be differentiated by their disruptive influence on the PVPA system. The results obtained are compared with explicit molecular dynamics simulations of lipid bilayers, AMPs, water and salt, where the motions of all individual water molecules relative to the lipid bilayer are monitored over the course of the simulations, allowing the calculation of theoretical apparent permeability constants of the corresponding single bilayer systems.

Proof-of-principle is presented that WIND-PVPA can be used to evaluate the lipid barrier destabilizing effect of active guest molecules by measuring changes in passive water- and ion permeabilities upon exposure. The method is highly flexible in terms of barrier composition, choice of probes and membrane active compounds.

## 1. Introduction

The escalation of multi-resistant bacteria, in combination with the low success rate of the discovery of new classes of antibiotics during the last decades, presents a dire threat to human health globally [1]. The need for new classes of antibiotics, as well as other treatment strategies, is ever increasing. On this background, the bacterial membrane has attracted increased attention as a drug target for several reasons. Firstly, there is limited development of resistance against antimicrobials that target the bacterial cell membrane [2]. Secondly, direct targeting of the cell membrane is a promising strategy to perturb non-growing, dormant infections and biofilms, where drugs targeting the bacterial metabolism are inefficient [3]. Thirdly, the development of many drug discovery hits with novel antimicrobial activities are discontinued due to inadequate permeability into the target bacteria, especially in the case of gram-negative bacteria, and thus targeting bacterial membrane permeability has emerged as a novel strategy in drug discovery [4].

One class of molecules with the capacity to directly target the cell membrane is antimicrobial peptides (AMPs). AMPs are a ubiquitous part of the innate immune defence in all living organisms, and they have been widely studied [5], with more than 3000 natural AMPs reported and characterized [6]. However, most natural AMPs are neither sufficiently potent, nor have suitable ADMET properties (absorption, distribution, mechanism, excretion, and toxicity) to be viable as commercial antibiotics for systemic (oral) administration. Over the last few decades, extensive effort has been put in to explore the potential of synthetic optimized AMPs to be developed into more realistic drug candidates.

One challenge in the rational design of AMPs is that drug discovery tools are traditionally not developed to deal with large, flexible molecules that target an amorphous target like a cell surface and act through diverse and poorly defined mechanisms. There is a lack of an in-depth understanding of AMP modes of action (MOA) and how to best optimize their activity since their MOA are diverse and often involve various types of self-aggregation on the bacterial membrane, needing to reach a

* Corresponding author.
*E-mail address:* johan.isaksson@uit.no (J. Isaksson).
[1] Shared authorship

https://doi.org/10.1016/j.bbamem.2022.183911
Received 22 December 2021; Received in revised form 23 February 2022; Accepted 5 March 2022
Available online 22 March 2022

local critical threshold concentration before efficacy is achieved [7]. The structural and physicochemical interplay between peptides and lipid bilayers needs to be characterized in order to determine the MOA of AMPs and optimize the activity of AMPs and other membrane-active compounds. An interesting interfacial activity model has been proposed with some success in unifying how the MOA of AMPs can be expressed [8]. The reviewed results therein identify that pore-forming peptides are exceedingly rare, and instead the overwhelming majority of AMPs does not form discrete pores in membranes, not even transiently, but instead causes bilayer leakage by a general disruption of membrane integrity. It is also noted that high peptide to lipid ratios used in vesicle-based leakage assays are prone to induce vesicle fusion, which in turn cause the release of the vesicle contents [8].

Hydration in general plays a vital role in lipid bilayer structure and function, for example, defining the stability of lipid vesicles in solution and controlling the permeability of small molecules across lipid bilayers [9]. Small uncharged molecules, including water, passively cross lipid bilayers with relative ease, which is necessary to maintain osmotic equilibrium while restricting the free diffusion of ions and large biomolecules. The topic is under some debate, but data suggests that the two dominating models can be used to describe water permeability – the solubility-diffusion model [10], and the transient pore formation model, the latter being more successful for describing the permeability of charged solutes [11]. In the rate-limiting diffusion step through the hydrophobic core of the bilayer, the diffusion is limited by available space, and hence the rate of diffusion is coupled to the order and motion of the lipid core, as solvated water and lipid molecules are dynamically linked to each other [12]. On a similar note, the rate of transient pore formation is expected to be higher in thinner and less ordered lipid phases. There is thus a link between lipid perturbation and increased permeability in both models [13].

Small cationic synthetic AMPs are known to associate near the lipid surface and both cause disorder in the lipid packing and pull down water molecules deeper towards the core of the lipid bilayer [14–15]. It is known that lipid bilayer hydration is associated with changes in lipid bilayer properties like increased permeability, increased area per lipid and reduced electric membrane potential. Small synthetic AMPs typically kill bacteria *via* what is traditionally described as a carpet model where peptides associate to-, and aggregate on, the membrane surface, where they give rise to a large imbalance in charge and surface tension between the outer and inner leaflet, eventually leading to a collapse of the membrane integrity [16]. Also, at concentrations lower than the critical concentration, the AMPs leads to membrane thinning, surface tension, clustering of anionic lipids and membrane deformation, all being physicochemical properties associated with increased permeability, loss of membrane potential and subsequent lysis [17]. It is also commonly observed that small synthetic AMPs exert an inhibitory effect on bacterial growth before they reach the critical Minimal Inhibitory Concentration (MIC) of fast membrane disruption. These observations, together with the role of membrane hydration and the bacterial membrane potential in permeability has sparked an interest in developing a simple assay to measure how the integrity of lipid bilayers is influenced by various AMPs or other guest molecules by quantifying the passive transport of ions and water across barriers composed of lipid bilayers.

As an alternative approach to vesicle leakage or vesicle swelling, we have explored the possibilities of measuring permeabilities across barriers constructed by immobilized phospholipid bilayer vesicle films on a solid membrane support. For this purpose, we have adapted an *in vitro* Phospholipid Vesicle-based Permeation Assay (PVPA) that was previously developed in our institute as an *in vitro* permeability model for passive drug transport through human biological barriers like intestine-, skin- and mucus membranes [18–21]. PVPA barriers are composed of a membrane filter support upon which liposomes with different size distributions and compositions are immobilized through cycles of centrifugation and freeze-thawing [18]. The resulting barriers are thus composed of layers of tightly packed vesicles on top of cellulose filter. Such barriers can be used to monitor the permeation of drugs from a donor to an acceptor compartment, which is subsequently quantified spectroscopically.

In the current study we have explored the possibility of using a modified version of the PVPA method, the Water/Ion NMR Detected-PVPA (WIND-PVPA), as a robust and straightforward way to measure to what extent guest molecules affect the membrane permeabilities of different entities, like ions, water molecules or other molecules of interest. The method was developed to study water and ion mobility over bacterial membranes in the context of bacterial membrane potential, but the method could be tailored to different contexts by studying the permeability of different molecules across different barriers.

## 2. Results and discussion

### 2.1. The PVPA model system

The PVPA model is an *in vitro* permeability model that is compatible with a wide array of molecular environments and barrier compositions (Fig. 1) [20–22]. In order to prove the principle of using the PVPA to probe for membrane disruptive activity of active AMPs, a model system composed by DMPC and DMPG was chosen. This composition has previously been successfully applied for the selection of active AMPs from combinatorial libraries [23]. In order to assess the effect of the surface charge of the lipid bilayers, the experiments were repeated in both pure DMPC (from here on referred to as **PC**) and 95% DMPC, 5% DMPG (*w/w*) (from here on referred to as **PC/PG**).

Ion and water transition across the barriers was monitored by solution NMR. A set amount of $D_2O$ (80% *v/v*) was introduced into the donor chamber, while the acceptor chamber contained only 0.5% $D_2O$ (for lock). Water transmission was subsequently quantified directly by $^2H$ NMR. In order to monitor ion transfer across the barrier, free EDTA was included in the acceptor chamber as a reporter molecule, while salts (100 mM $CaCl_2$ and 100 mM $MgCl_2$) were added to the donor chamber and the emerging proton resonances of the EDTA-$Ca^{2+}$ and EDTA-$Mg^{2+}$ complexes in the acceptor chamber were quantified using $^1H$ NMR. Transitioned ions form strong complexes with EDTA, which gives rise to unique and stable non-overlapping proton signals for the ion complexes, which can be used to identify and quantify the ion complexes individually [24]. This allows for parallel monitoring of both $Mg^{2+}$ and $Ca^{2+}$ in a single pot experiment provided there is unbound EDTA in excess (Fig. S1 in the SI). The cumulative amounts quantified from the integration of the $^1H$ and $^2H$ resonances in the acceptor solutions were plotted *versus* time to visualize the permeability profiles, and the apparent permeability constants ($P_{app}$) were calculated according to Eq. (1) (See Materials and methods).

The potential to use the PVPA to measure changes in permeability as a function of exposure to various guest molecules has been evaluated using four synthetic peptides (compounds **1–4**) and TritonX-100 (**5**) as a positive control for membrane disruption (Fig. 2). KP-76 (**1**), AMC-109 (**2**) and cyclic hexapeptide cWRWRWR (**3**) are established synthetic AMPs with known MIC values (inserted table in Fig. 2) that have been selected for their different activities despite their chemical similarity [25–26]. From this set, AMC-109 (formerly LTX-109) is an AMP with a MOA that targets the bacterial cell wall. AMC-109 is currently in phase IIA trials for treatment of topical infections [27]. Due to poor solubility of AMC-109 in the donor buffer, owing to the high concentration of salts, only $D_2O$ transmission data was acquired for AMC-109 [25–26]. The RAR peptide was selected for its chemical similarity to both KP-76 and AMC-109, while it is neither interacting with lipid bilayers nor possessing any antimicrobial effect because of its lack of hydrophobic bulk (unpublished results). Triton (2% *w/v*), used as positive control, is known to effectively lyse cell membranes and to be efficient at solubilizing PC lipids [28]. In the PVPA, Triton is observed to increase the water permeability across both **PC** and **PC/PG** barriers by approximately 50% [28].

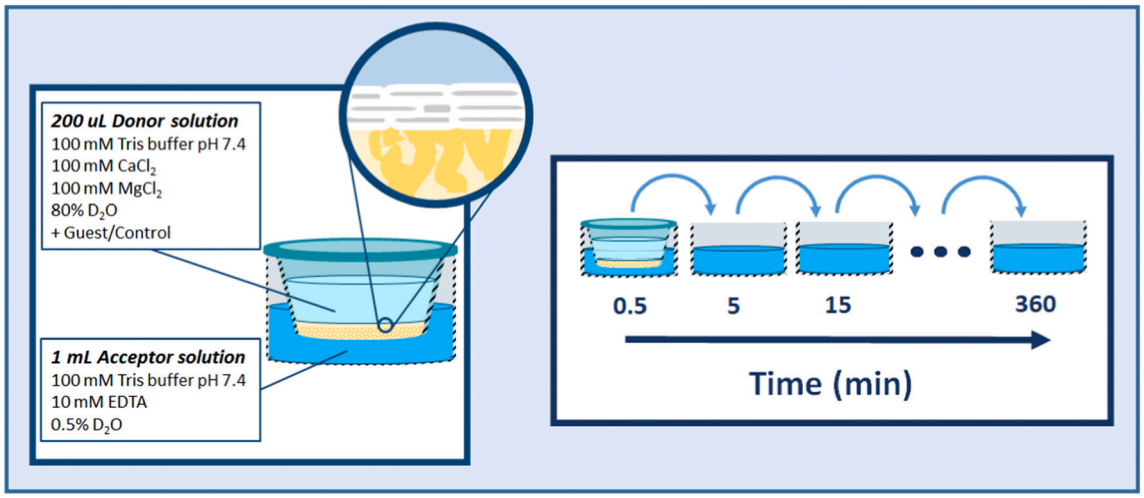


**Fig. 1.** Experimental setup of the PVPA model in which phospholipid vesicles are packed on top of a porous cellulose support strip that is attached to a plastic insert. The insert houses the donor solution which contains the guest molecule and is placed in a well of acceptor solution for increasing intervals of time.

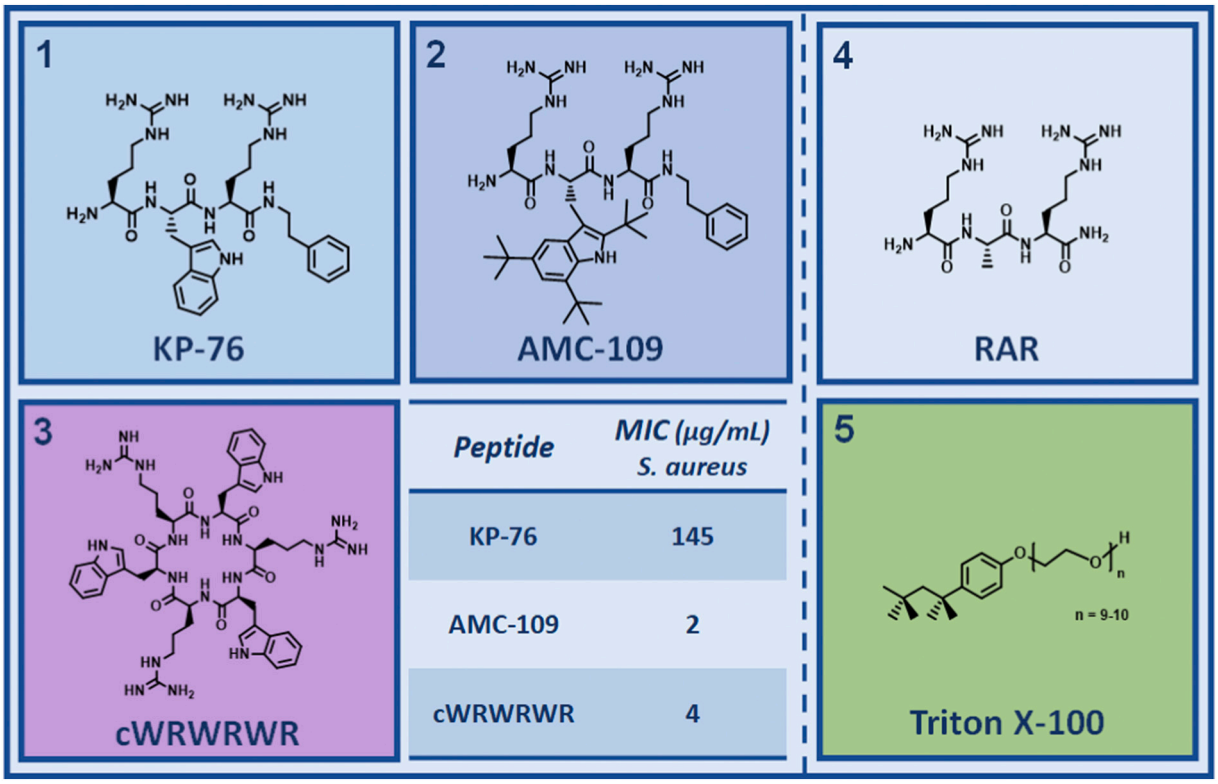


**Fig. 2.** Chemical structures of compounds (1) **KP-76** (RWR-NHPh) [26], (2) **AMC-109** (RTBtR-NHPh) [29], (3) **cWRWRWR**, (4) **RAR** and (5) **TritonX-100**. Minimum inhibitory concentration (MIC) for *S. aureus* strain ATCC 25923.

In order to show that the PVPA model can be used to evaluate the lipid bilayer integrity in response to external factors, the $D_2O$ transmission across the barriers was quantified under different salt concentrations, lipid compositions, and in the presence of different AMPs.

### 2.2. Salt influence

The permeability of water and solutes across any semi-permeable barrier is known to be affected by several factors, *i.e.* the osmotic pressure, hydrostatic pressure difference and concentration differences of the solute in question – as described by the Kedem-Katchalsky equations [30–31]. In the PVPA experimental setup, the addition of salt on one side of the barrier gives rise to a net osmotic pressure on the semi-permeable barrier. This will drive water molecules against the salt gradient, since water crosses lipid bilayers more easily than ions. The ions also exert a concentration driven flux from the donor to the acceptor chamber, which is expected to also affect the water flux in the system. Salt is furthermore known to potentially affect the ordering and structure of the lipid bilayers themselves [32–33]. Therefore, the basic influence of the salt concentration on $D_2O$ transmission across the **PC/PG** barriers in the PVPA setup was first controlled by a series of blank experiments with increasing equimolar concentrations of $MgCl_2$ and $CaCl_2$ (Fig. S1 in the

Supporting information).

As expected, the measured rate of $D_2O$ transmission decreased with increasing total salt concentration, as more water is retained on the donor side through osmotic pressure. The combined effect of salt presence on the system is hard to predict accurately for different systems, and Fig. S1 illustrates the importance of running blanks using identical lipid and salt concentrations, as well as other potential additives like for example DMSO as a solubility enhancer. There are no indications that the method does not tolerate salt concentrations up to 200 mM, thus allowing the acquisition of water and salt permeability data in a one-pot experiment if the appropriate blank is used.

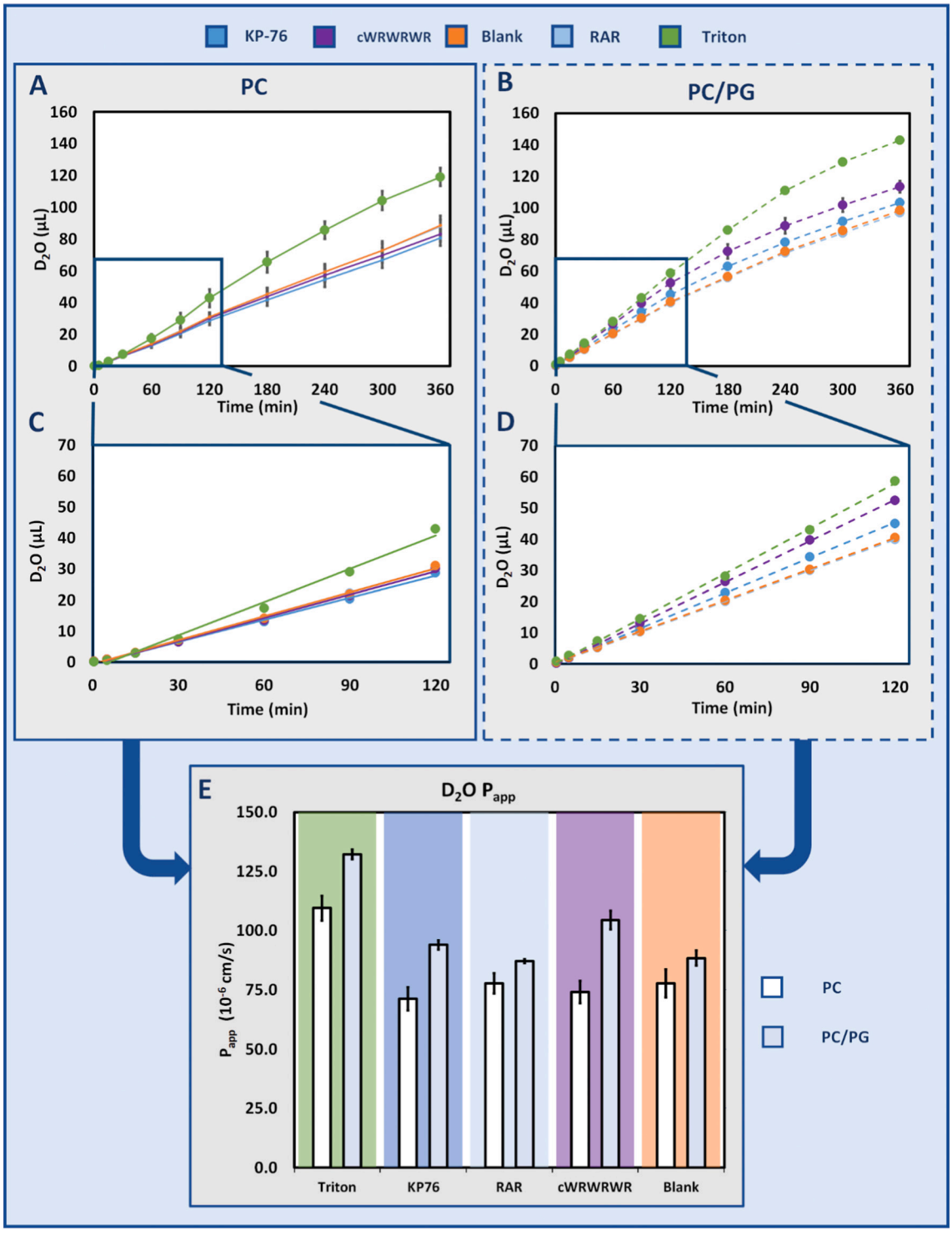


**Fig. 3.** Summary of the changes in the water permeability in the presence of antimicrobial peptides (**KP-76** and **cWRWRWR**,), negative control (**RAR**), positive control (**Triton**), or in the absence of any guest molecules (**blank**). The cumulative volume of $D_2O$ transmitted across **PC** barriers was plotted against the 6 h experiment time acquired across (a) uncharged **PC** barriers and charged (b) **PC/PG** barriers. The respective initial slopes are expanded in (c) and (d). The apparent permeability constants ($P_{app}$) calculated from the initial slopes are summarised in (e). Error bars represent the standard deviation of the three replicates.

### 2.3. Water transmission

The permeability of water was tested for two lipid compositions – the **PC** and the **PC/PG**. In the **PC** barriers, the tested peptides showed little to no effect on the water transmission compared to the blank, with only Triton significantly increasing the permeability of water (Fig. 3 A, C). The abundance of negatively charged lipids on the surface of bacteria and cancer cells is known to be a selectivity factor for many antimicrobial/anticancer peptides, and the observed lack of membrane destabilization could potentially be attributed to the lack of any negative net charge on the lipid barrier surface. It is worth noting that this observation alone would not rule out other causes, like for example the overall quality of the lipid packing, or vesicle fusion on the membrane support being more efficient in the absence of charge.

There was a consistent trend that the baseline transmission of $D_2O$ across the barrier is increased when PG was present. This increase is observable in all tested samples, most evidently by the blank and the control peptide. Comparison of the controls showed an ~15% increase in water transmission for Triton and the blank with the introduction of DMPG.

Interestingly, significant additional reductions in barrier integrity were observed for the active peptides with the introduction of a negatively charged component to the barriers. The addition of 5% PG lipids allows favourable electrostatic interactions between the positively charged peptides and the negatively charged lipids, which was reflected in the AMPs significantly reducing the integrity of the lipid barrier in the assay (Fig. 3 B, D). The cyclic cWRWRWR (**3**) increased the $P_{app}$ of water from 74 to 104 $\times$ $10^{-6}$ $cms^{-1}$ (~40%) across the **PC/PG** barrier compared to the **PC** barrier, which was close to the $P_{app}$ increase caused by Triton treatment. Similarly, the presence of charged lipids enabled also the moderately active peptide, KP-76 (**1**), to increase the permeability across the barrier from 71 to 94 $\times$ $10^{-6}$ $cms^{-1}$ (~30%). The negative control peptide, RAR (**4**), had no observable effect on the $P_{app}$ of $D_2O$ across neither the **PC** nor the **PC/PG** barriers compared to the control.

AMC-109 (**2**) was not soluble in the salt concentration used in the one-pot experiment, thus only the water permeability was assessed in the absence of salt across **PC** barriers (Fig. 4). Even though the peptide possesses a low MIC value of 2 μg/ml, there is no detectable effect on the water permeability under these experimental conditions. This will be further discussed together with the computer simulation results below.

### 2.4. Ion transmission

Ion transmission was monitored by $^1H$ NMR using EDTA as a reporter molecule. EDTA has a strong affinity for divalent ions and forms stable complexes with unique chemical shifts with both $Mg^{2+}$ and $Ca^{2+}$. Comparison of $Ca^{2+}$ and $Mg^{2+}$ $P_{app}$ (Fig. 5) shows that the $P_{app}$ and total transmission for $Mg^{2+}$ was consistently higher than for $Ca^{2+}$. This observation was in line with the expectation that the smaller size of the $Mg^{2+}$ ions would allow them to more easily cross the barrier. It is noteworthy that there is a lag-phase before permeated ions can be detected that is not present for water. However, overall the ion permeability reflects the same pattern as for the water permeability above. In pure **PC** barriers there is no observed increase of permeability upon treatment with KP-76 (**1**), AMC-109 (**3**) and RAR (**4**), while in the **PC/PG** barriers there is an increase in ion leakage reflecting the ranking of the MIC values of the peptides; the most active compound, cWRWRWR (**3**), showed the largest increase in ion permeability. While the relative changes in the $P_{app}$ of ions are consistent with the respective $D_2O$ transmissions, there are some significant deviations.

The ion permeability did not change significantly upon the introduction of charged lipids as was the case for water permeability (compare Figs. 3e and 5e). This suggested that the overall increase in water permeability observed for the **PC/PG** barriers over the **PC** barriers was not just a potential effect of imperfect lipid packing onto the cellulose support caused by anionic repulsion. This was also supported by both barriers having near identical electric resistance and calcein permeability (Supp Table S1).

With respect to the effect of peptide exposure, a stronger relative impact on ion transmission is observed for cWRWRWR (**3**) in **PC/PG** barriers compared to the respective $D_2O$ transmissions. The ion $P_{app}$ is increased two-fold in the presence of charge, while only a 40% increase is observed for $D_2O$. This behavior is not observed for KP-76 (**1**), where there is no observed increase in salt permeability. This difference in response indicates that there is difference in how KP-76 (**1**) and cWRWRWR (**3**) interact with the lipid barriers, and particularly in how cWRWRWR (**3**) facilitates ion transport across the barrier.

The full time resolved permeability curve further reveals differences in behavior of the different guest molecules. The initial transmission rate of ions is higher for cWRWRWR (**3**) than that of Triton (**5**), but over time the rate in the presence of Triton (**5**) steadily increases to the point that it overtakes the permeabilizing effect of cWRWRWR (**3**) after 240 min

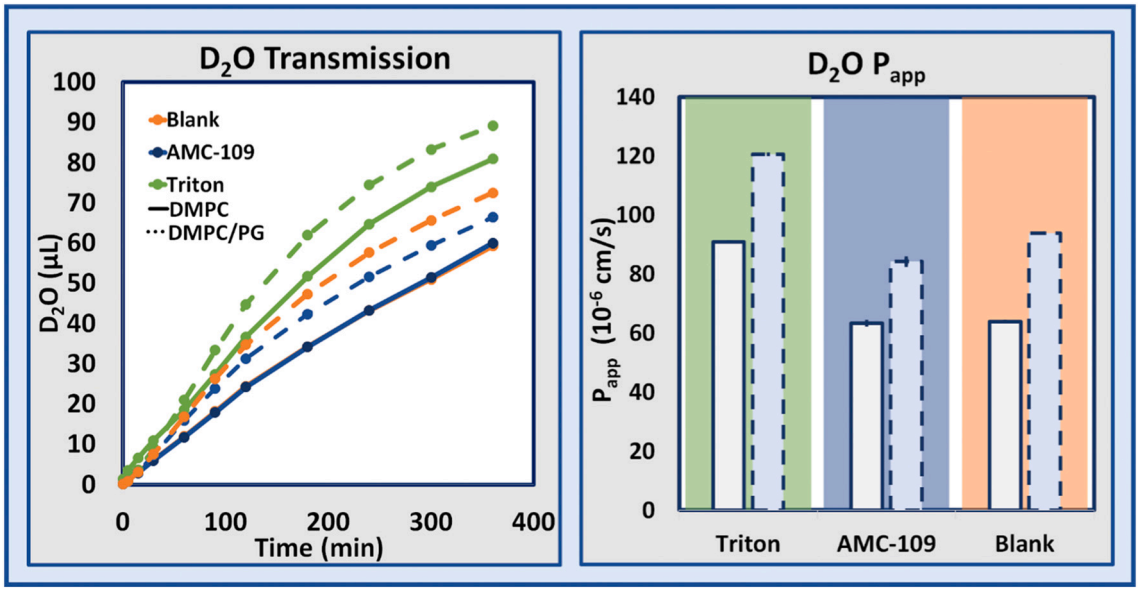


**Fig. 4.** Water permeability of AMC-109 (**2**) across PC barriers in no salt conditions. Left – The cumulative volume of $D_2O$ transmitted across **PC** (solid lines) and **PC/PG** (dashed lines) barriers. Right - The apparent permeability constant ($P_{app}$) calculated from the initial slopes.

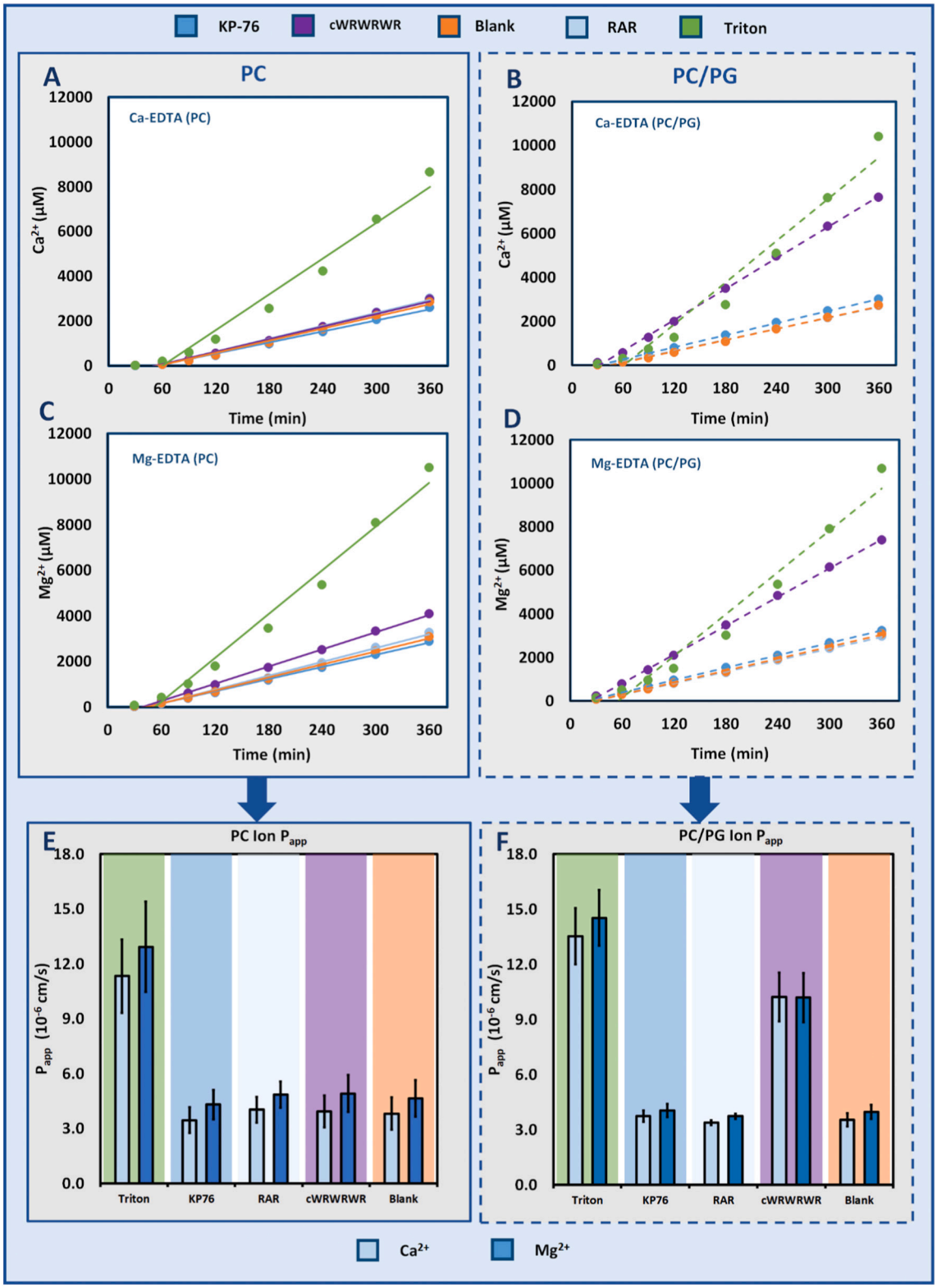


**Fig. 5.** The observed changes in the permeability of $Ca^{2+}$ and $Mg^{2+}$ in presence of antimicrobial peptides - KP-76 (**1**), cWRWRWR (**3**), controls RAR (**4**), Triton (**5**), and blank, across both **PC** and **PC/PG** barriers. The top graphs show the cumulative concentration of $Ca^{2+}$ transmitted across (a) **PC** and (b) **PC/PG** barriers during the 2 first hours of the experiment. The middle panels show the corresponding plots for $Mg^{2+}$ across (c) **PC** and (d) **PC/PG** barriers. The solid line presents the linear fit of the seven data points in this period. The bottom panel summarizes the calculated $P_{app}$ of $Ca^{2+}$ and $Mg^{2+}$ across the (e) **PC** and (f) **PC/PG** barriers. Error bars represent the standard deviation of three replicates.

(Supp Fig. S2). The accelerating effect on the $P_{app}$ by Triton (**5**) exposure suggests that Triton (**5**), unlike the AMPs, exerts a continuous dissolving effect on the lipids that make up the barriers.

Based on the permeability measurements alone it is difficult to make any detailed conclusions about how the different lipid compositions and AMP interactions affect the water- and ion permeabilities. To increase our understanding of the studied systems we have therefore complemented the permeability experiments with a computer simulation setup to that allows the quantification of membrane hydration, water permeability, lipid disorder and bilayer thickness in the presence of AMPs.

### 2.5. Molecular modelling

Explicit atom calculations of biomembranes are computationally demanding, hence two of the peptides, KP-76 (**1**) and AMC-109 (**2**), were selected for detailed computer simulations. Data analysis protocols were setup to analyse the effect of the antimicrobial peptides on the lipid bilayer integrity, and to explore the behavior of the water in the presence and absence of AMPs. The simulations were setup using explicit lipid molecules in the two lipid compositions used in the assay – 100% DMPC (**PC**) and 95% DMPC/5% DMPG (**PC/PG**). Simulations were then performed in the presence of 0, 4 or 8 peptide molecules per 336 lipid molecules, in triplicates with different seeds over a total of 600 ns. The analysis was started after 5 ns of simulation to ensure the system was in an equilibrated state throughout the trajectory.

To track water molecules crossing the bilayer, a script was written to select all water molecules that during the simulation entered the hydrophobic core of the bilayer (see experimental section for details). The selected waters were then recorded throughout the trajectory to distinguish between molecules crossing and exiting the bilayer at the opposite side (Fig. 6b) from the ones merely entering and returning to the bulk water on the side they came from (Fig. 6a).

First, the two lipid compositions were simulated without any guest peptides to establish the baseline passive water permeability in the two models. Analysis of the water molecules revealed that over the course of 195 ns, 30 ± 6 and 36 ± 7 water molecules crossed the bilayer for **PC** and **PC/PG** respectively. There were no major events observed for the lipid bilayer on the studied time scale, but water molecules were instead passively diffusing through, distributed over the whole trajectory. The simulation time is expected to be too short to observe events like transient pore formation taking place with any probability, but long enough to allow the observation of water molecules crossing through passive diffusion (see Fig. 6b for a representative trajectory in pure lipids and Supplementary for all analysed trajectories).

The observed simulated rates correspond to a theoretical permeability constant of $2.2 \pm 0.4$ and $2.6 \pm 0.5 \times 10^{-3}$ cm/s for the two lipid compositions respectively.

Bilayers of the two lipid compositions were then challenged with exposure to 4- or 8 AMP molecules, corresponding to 1:84 and 1:42 peptide:lipid ratio respectively. That places the concentration in a range below the MIC values that report rapid killing of bacteria through membrane-cataclysmic events. The effects on the lipid bilayer order and thickness, as well as the water permeability, were examined for signs of general destabilization that could explain bacteriostatic effects below the MIC of rapid cell disruption.

With respect to the two lipid compositions used, the overall result was that the number of water molecules penetrating the bilayers was similar (Fig. 7a). Experiment suggests that water penetrates the **PC/PG** barriers slightly more efficiently than the pure PC barriers, and this is also the weak trend observed in the simulations, though the sampling was insufficient to identify any statistically significant differences in permeability (Fig. 7b).

The statistically significant observation that could be made from the water counts was that the presence of 8 molecules of KP-76 (**1**) increased the number of water molecules that successfully penetrated deep into the bilayer (Fig. 7a). However, it was qualitatively observed that peptides penetrating down into the bilayer often pulled water molecules with them, increasing the overall hydration of the hydrophobic core. In order to visualize the total hydration of the bilayer core, the time each water molecule spent in the $-5 < Z < 5$ range was integrated over each trajectory (Fig. 7c). The hydration plot displayed a clear trend that more

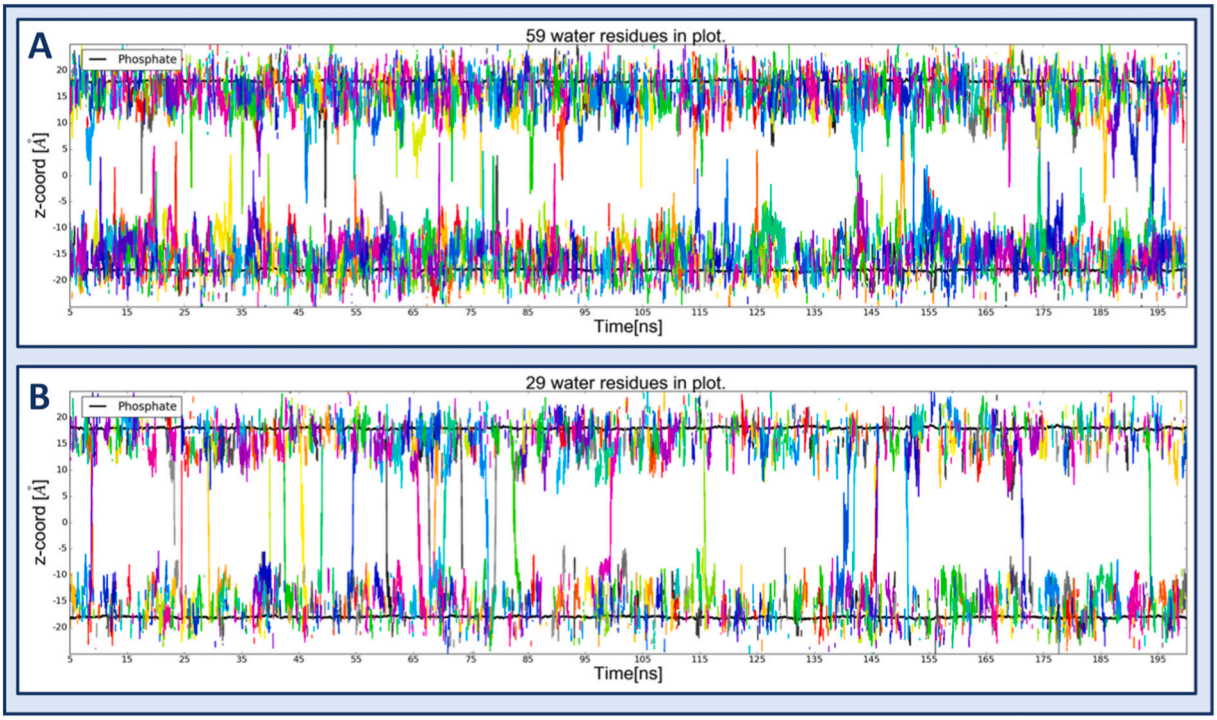


**Fig. 6.** Representative plot of selected water molecules that either enter the hydrophobic core and return to the bulk water of the same side (a) or that cross the bilayer and exit on the opposite side (b). Each color represents one unique water molecule.

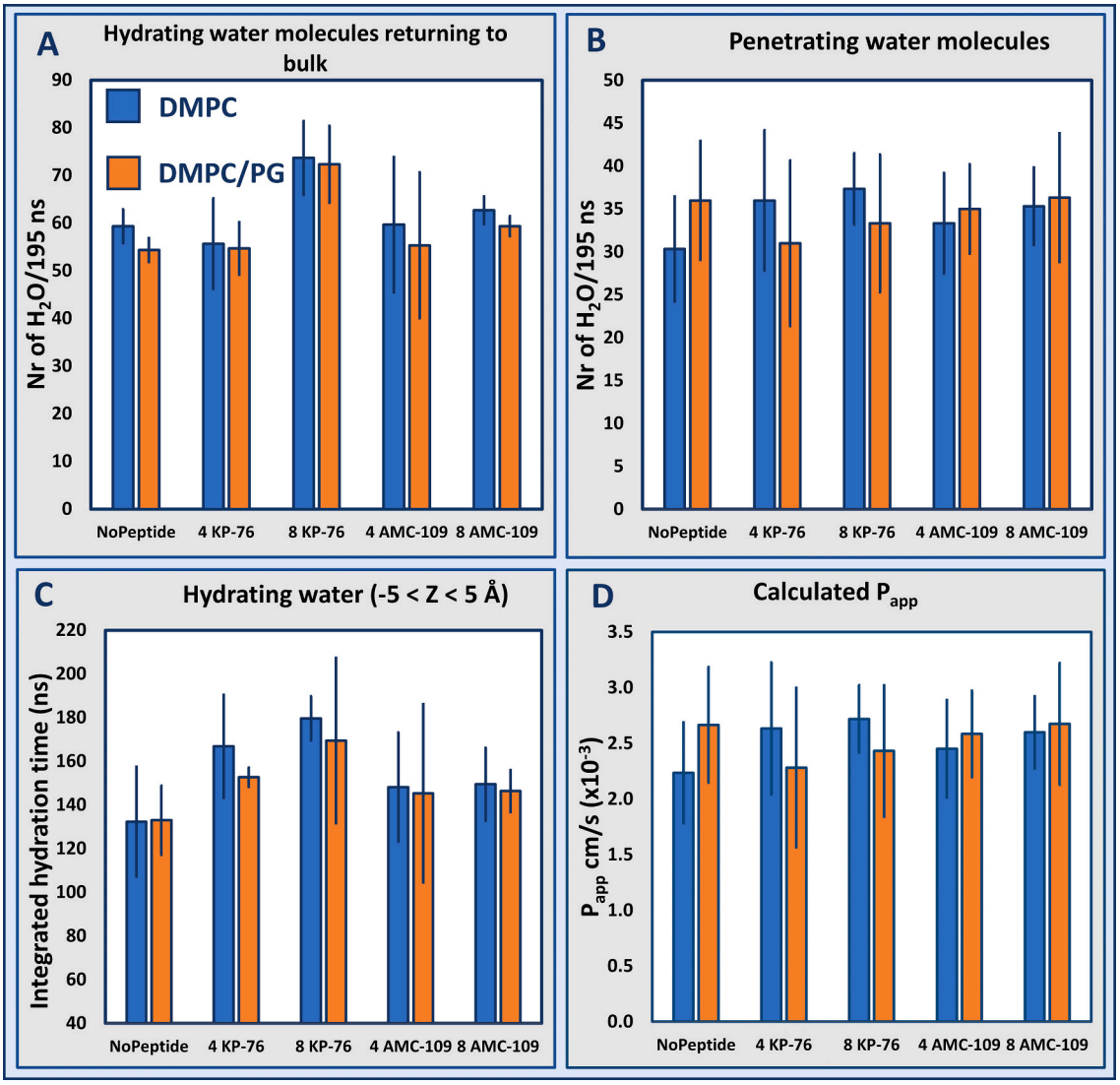


**Fig. 7.** Diagram showing the raw number of water molecules that enter the lipid bilayer during the simulations and then either (a) return to the bulk water or (b) cross the bilayer. In (c) the time of all water molecules spent within 5 Å of the middle if the bilayer is integrated to represent the overall hydration of the hydrophobic core. For completeness, (d) shows the simulated $P_{app}$ calculated from the permeation counts in (b). Simulations have been performed in using either **PC** (blue) or **PC/PG** (orange), and in the presence of 4 or 8 KP-76 (**1**) or AMC-109 (**2**) (formerly LTX-109) respectively. (For interpretation of the references to color in this figure legend, the reader is referred to the web version of this article.)

water resides longer in the bilayer when more KP-76 (**1**) is added to the simulations - this is true in both compositions. Thus, while these simulations were not sufficiently long and did not include a sufficiently high peptide:lipid ratio to reproduce a statistically significant increase in the permeating water molecules count, they could show that the water molecules that entered the bilayer stayed there for a longer time, and therefore the total water content in the lipid bilayer over time increased significantly.

AMC-109 (**2**) did not cause any increase in water permeability or hydration in the simulations, which is in agreement with the lack of effect observed in the WIND-PVPA, despite AMC-109 (**2**) being a potent AMP able to disrupt bacterial cell walls at critical peptide:lipid ratios. Inspection of the simulations quickly revealed that AMC-109 (**2**) was prone to self-aggregate instead of penetrating into the lipid bilayer, explaining the lack of observable effect (Fig. 8) *versus* lipid compositions with a low charge density. This had the effect that for the majority of the time, AMC-109 (**2**) had no contact surface with the lipid bilayer, and hence did not significantly reduce the bilayer integrity.

## 3. Conclusion

The effect of three antimicrobial compounds on the permeability of zwitterionic lipid barriers has been compared in the presence- (**PC/PG**), and absence (**PC**), of negative charge for three anti-microbial peptides: KP-76 (**1**), AMC-109 (**2**) and cWRWRWR (**3**). KP-76 (**1**) has a modest MIC value, whereas AMC-109 (**2**) and cWRWRWR (**3**) both possess potent anti-microbial activities, reflected by MIC values of 2 μg/ml and 4 μg/ml against *S. aureus* respectively (Table 1).

Interestingly, none of the peptides had any statistically significant effect on the barrier integrity in the absence of negatively charged lipids, but as soon as a small fraction of charge was introduced (5% PG) a destabilizing effect of the peptide interactions began to emerge. KP-76 (**1**), cWRWRWR (**3**), and RAR (**4**) followed the expected trend according to their respective activities, where the modestly active KP-76 (**1**) results in a small but statistically significant increase in water permeability across the barrier with 5% positive charge (**PC/PG**), while the more potent cyclic peptide had a pronounced effect on the permeability, and especially on the ion permeability which saw a twofold increase in permeability compared to the blank. These observations are in line with

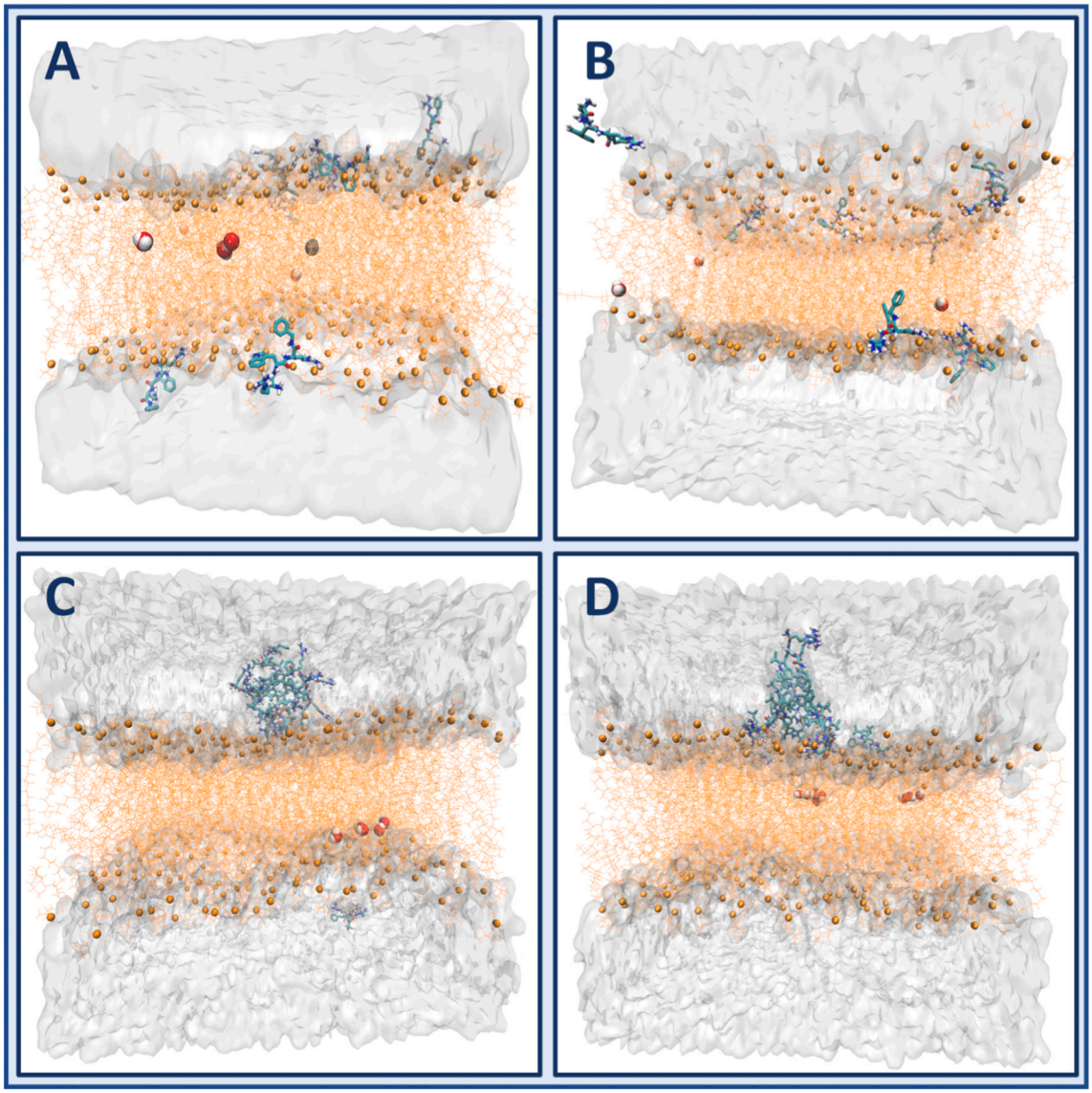


**Fig. 8.** Representative snapshots of the simulation of 8 molecules of KP-76 (**1**) in (a) **PC** and (b) **PC/PG** bilayers, compared to 8 molecules of AMC-109 (**2**) in (c) **PC** and (d) **PC/PG** bilayers. AMC-109 (**2**) displayed a clear tendency to self-aggregate and to stay in these aggregates during the simulation time.

this class of peptides displaying a selectivity for negatively charged surfaces of bacterial- and cancer cells over the neutral surface of healthy eukaryotic cells [34–35].

The most active peptide, AMC-109 (**2**), did however behave unexpectedly in the assay, not displaying any effect on the permeability of neither the **PC** nor the **PC/PG** barriers. The computer simulations provided a plausible explanation as to why AMC-109 (**2**) did not damage the integrity of the barriers, as AMC-109 (**2**) was prone to spontaneously self-aggregate and form stable micelle-like structures in the simulations. This could potentially serve as a reservoir for peptide molecules and contribute to a more pronounced threshold concentration and selectivity towards bacterial cells with a high negative charge density. This behavior of AMC-109 (**2**) is being thoroughly investigated elsewhere (personal communication Wouter H. Roos). This highlights the importance of supporting experiment with simulations or orthogonal methods. Together these results give us a glimpse of the mode of action of this class of antimicrobials, where solubility, local concentrations and peptide to lipid ratios are central to the anti-microbial effect.

The proposed WIND-PVPA method has some characteristics that need to be recognized. The barriers are not a single bilayer, but rather a stack of packed unilamellar vesicles. As such, the *absolute* values of the apparent permeabilities through the barriers ($10^{-6}$ cm/s range for water) are expected to be significantly different from the *absolute* permeabilities through single bilayers ($10^{-3}$ cm/s range for water) [36] as the barriers are several orders of magnitude thicker than a monolayer. Therefore, the WIND-PVPA should be used to assess the relative response to membrane disrupting- or dissolving stress. There are also indications of that PVPA barriers inherently can have microscopic hydrophilic pathways contributing to the total permeation. In the original PVPA, the barrier leakiness is assessed by measuring the calcein permeability – a large polar molecule with low permeability. The quality criterium for "tight" barriers is that the calcein permeability is $<10^{-7}$, whereas the native calcein permeability across a single bilayer is expected to be in the $10^{-11}$ range from literature reported liposome leakage [37]. Therefore, it is not possible to determine the actual mechanisms behind permeabilities that are lower than $10^{-7}$, which is the case for both calcein and sodium ions.

The concentrations used in the assay were 4 mg/ml, which is high with respect to the MIC values of these peptides. However, at the same time the peptide:lipid ratio was approximately 1:10, which is in a range that will normally induce destabilization of vesicles, but is low with the respect to the peptide:lipid ratio used in MIC assays, which can be as

**Table 1**
Summary of $P_{app}$ determined for all tested guest molecules in PVPAs with both lipid compositions.

| | MIC (μg/mL) | DMPC ($P_{app}$ x $10^{-6}$ cm/s) | | | DMPC/PG ($P_{app}$ x $10^{-6}$ cm/s) | | |
|---|---|---|---|---|---|---|---|
| | *S. Aureus* | $Ca^{2+}$ | $Mg^{2+}$ | $D_2O$ | $Ca^{2+}$ | $Mg^{2+}$ | $D_2O$ |
| KP-76 | 145 | 3.5 ± 0.7 | 4.3 ± 0.8 | 71 ± 4.9 | 3.7 ± 0.3 | 4.0 ± 0.3 | 94 ± 2.0 |
| AMC-109[a] | 2 | – | – | 63 ± 0.6 | – | – | 84 ± 1.2 |
| cWRWRWR | 4 | 3.9 ± 0.9 | 4.9 ± 1.0 | 74 ± 4.7 | 10.2 ± 1.3 | 10.2 ± 1.3 | 104 ± 3.9 |
| RAR | – | 4.0 ± 0.7 | 4.9 ± 0.7 | 78 ± 4.2 | 3.4 ± 0.1 | 3.7 ± 0.1 | 87 ± 0.8 |
| Triton | – | 11.3 ± 2.0 | 12.9 ± 2.5 | 109 ± 5.3 | 13.5 ± 1.5 | 14.5 ± 1.5 | 132 ± 2.1 |
| Blank | – | 3.8 ± 0.9 | 4.7 ± 1.0 | 78 ± 5.9 | 3.5 ± 0.4 | 4.0 ± 0.4 | 88 ± 3.1 |

[a] Conducted in the absence of $CaCl_2$ and $MgCl_2$ - No increase observed relative to the blank.

much as 1000:1 due to the low cell density in the assay [8]. It is also expected that the outermost bilayers will experience higher local concentrations of guest molecules than the deeper layers will, and hence could potentially experience cataclysmic events if the guest molecule has disruptive properties. The batch consistency also needs to be considered. It's important to routinely probe the zeta potential and calcein permeability of every new batch (see Methods). If these factors are under control, WIND-PVPA offers a unique method to monitor *changes* in membrane permeability that is straightforward to setup, can be tailored to different scientific questions and can potentially be scaled up and automated for screening.

We herein show the proof of principle that the WIND-PVPA method can be used to assess the influence of AMPs and other membrane active molecules on the integrity of lipid-based barriers. WIND-PVPA as a method is easy to use and is very flexible in its application. The barriers themselves can be designed to mimic any microbial- or physiological barrier by using different lipid compositions, lipid- or cell wall isolations. The experiment can also be modified to monitor different entities, for example other salt/reporter pairs, size markers, biomarkers or isotopes. The core experiment can thus be tailored to provide data on different scientific questions, including integrity, permeability, selectivity and mode-of-action. The core methodology is currently being developed in multiple directions outside the scope of this work.

## 4. Materials and methods

All common chemicals are of analytical purity and supplied by Merck KGaA, Darmstadt, Germany. All the lipid samples had been supplied by Avanti Lipids (Alabaster, Alabama, US).

### 4.1. Preparation of PVPA barriers

PVPA barriers were prepared following a modified method from Flaten et al., (2006) [18]. Briefly, DMPC (**PC**) or DMPC:DMPG (5% DMPG, *w*/w) (**PC/PG**) liposomes were prepared *via* the thin film hydration technique, and the PVPA barriers were prepared by depositing either **PC** or **PC/PG** liposomes on top of nitrocellulose membrane filters (pore size 650 nm) and by immobilizing them by cycles of heating at 50 °C. The liposomes utilized for the preparation of the PVPA barriers were manually extruded through 800 nm filters prior to their addition on top of the membrane filters. To prepare for further use, the PVPA barriers were thawed at 50° C for 45 min, or until dry. Integrity of barriers was tested by calcein permeability assay and electrical resistance (Supp Table S1).

### 4.2. WIND-PVPA

The WIND-PVPA experiment consists of a donor and receiver chamber separated by a lipid barrier. The experiment has been done in 24 well plates, which served as a series of receiver chambers. The donor chamber is part of the barrier and can be moved freely from well to well. After the addition of the sample solution to the donor chamber, the barrier was moved from well to well in series of time points – 0.5, 5, 15, 30, 60, 90, 120, 180, 240, 300, 360 min and one overnight sample. The donor chamber contained 200 μl of 100 mM Tris buffer pH 7.4, 100 mM $CaCl_2$, 100 mM $MgCl_2$, the tested peptide (4 mg/ml) or Triton (2% *w/v*) in 80% $D_2O$ (Merck KGaA, Darmstadt, Germany) and 20% MiliQ water. The receiver chamber contained 1 ml of 100 mM Tris buffer pH 7,4 and 10 mM EDTA in 0.5% $D_2O$ and 99.5% MilliQ water. Afterwards, both donor and acceptor solutions were transferred to 5 mm short NMR tube for NMR measurement. The transition experiment was completed at 20 °C (controlled room temperature). Due to poor solubility in the presence of the salts, the AMC-109 (**2**) WIND-PVPA used a 10 mM Tris buffer pH 7.4 without salts in the donor chamber, nor EDTA in the acceptor chamber – all other aspects of the experimental setup remained the same.

The apparent permeability coefficient ($P_{app}$) was calculated for water and both $Mg^{2+}$ and $Ca^{2+}$ ions from Eq. (1) derived from Fick's law:

$$P_{app}\left(\frac{cm}{s}\right) = \frac{dQ}{dt}*\frac{1}{A*C_d} \quad (1)$$

where dQ/dt is transition speed of $D_2O$ (μl/min) or ions (μmol/min), A is surface area of PVPA barriers ($cm^2$) and $C_d$ is volume of water (μl) or concentration of ions (μM) in donor compartment.

### 4.3. NMR acquisition

NMR spectra were acquired on a Bruker Avance III HD spectrometer operating at 600 MHz, equipped with an inverse TCl cryo probe. All NMR spectra were acquired at 298 K using 5 mm tubes using standard pulse programs for acquisition in Topspin 3.5pl7 (Bruker BioSpin, Germany). Spectra were processed automatically using TopSpin 4.0.8 (Bruker, Germany) and Matlab R2020b with Signal processing and Bioinformatics toolbox (USA, MA, Natick). The processing scripts are available at https://github.com/MarJakubec/TopSpin-Matlab-Processing.

The integrals of the $D_2O$ peaks were adjusted *via* subtraction of the baseline level of $D_2O$ present in the acceptor solution. The cumulative adjusted integrals were converted to volume using a calibration curve and plotted against time. The slope of the line consisting of the points that made up the first 2 h for each series was calculated and plotted. The same process was repeated for EDTA using the peaks between 2.42 - 2.48 ppm, and 2.56–2.61 ppm respectively for $Ca^{2+}$ and $Mg^{2+}$ to yield the concentration of each ion.

### 4.4. Computational details

The AMPs, KP-76 (**1**) and AMC-109 (**2**) (formerly LTX-109) were used in the molecular dynamics (MD) simulations [25–26]. The molecular models of the synthetic AMPs were built with Maestro (Schrödinger Release 2021–4: Maestro, Schrödinger, LLC, New York, NY, 2021). The topology and parameters where generated using the automatic CGenFF program ParamChem [38] The resulting atomic charges were compared to charges of similar residues in the CHARMM36 All-Hydrogen Topology File for Proteins as well as the general CGenFF topology File [39]. Two lipid bilayers were built using the CHARMM-

GUI membrane builder [40]. One consisting of 336 DMPC lipids (**PC**), the other having 319 DMPC lipids and 17 DMPG lipids to give a 95% DMPC/5% DMPG bilayer (**PC/PG**). Both bilayer systems have an ion concentration of 100 mM $MgCl_2$ and 100 mM $CaCl_2$. The **PC/PG** bilayer has an additional 17 sodium counter-ions due to the negative charge of DMPG lipids. The lipid bilayers were calibrated for 30 ns. Further, VMD [41] was used to prepare 4 systems for each of the calibrated **PC**- and **PC/PG** bilayer, containing 4 and 8 molecules of KP-76 (**1**) and AMC-109 (**2**) respectively. For systems with AMPs, $Cl^-$ was added as counter-ions to the positively charged AMPs. Water molecules within the hydrophobic region of the lipid bilayer were removed. The same procedure was applied to the **PC** and **PC/PG** bilayer systems not containing AMPs, which were used for further simulations. Three parallels of each system were then simulated for 200 ns. The NAMD software package [42] was used for the MD simulations, which were performed under periodic boundary conditions in the NpT ensemble. The CHARMM36 All-Hydrogen Lipid Parameters [43] were used for the lipids. Water was modelled using the TIP3P model and the geometry of the water molecules was constrained using the SHAKE algorithm (36). A target pressure of 1 atm [44] was obtained using the Langevin piston method (34), with an oscillation period of 100 fs and damping time scale of 50 fs. Langevin dynamics was used to control the temperature at the physiological temperature 310 K, with a damping coefficient of 1 $ps^{-1}$ [45]. The Particle Mesh Ewald (PME) method was applied for long-range electrostatic forces [46]. Further, the bonded forces were evaluated every 1 fs, short-range none-bonded forces every 2 fs, and long-range electrostatics every 4 fs. A smooth cut-off was used between 8 and 10 Å.

### 4.5. Data analysis

The simulated systems had the lipid bilayer oriented in the xy-plane with the z-axis perpendicular to the membrane surface. Before analysis, the frames of the trajectory were placed with the membrane centre of mass at x-, y- and z = 0.

Permeability of water and ions as well as the saturation of the membrane models was examined. The z-coordinates of water oxygens or ions within a given distance of the lipid bilayer hydrophobic core were extracted every frame (5 ps steps) of the 200 ns MD simulation trajectory. The resulting water molecules or ions were considered further if they were present 2 frames or more. The z-coordinates of a given water molecule or ion were then tracked to see if the residue would permeate the lipid bilayer or return to the bulk water from where it entered. In addition to counting the number of water molecules that cross the centre of the bilayer, the overall time which water molecules spent within 5 Å of the bilayer centre was accounted for. Further, water molecules which crossed the centre of the lipid bilayer were examined to see if during the simulation they were within 8 Å of the peptides simultaneously to the selected hydrophobic core. The z-coordinates were extracted every frame the water residues were in both the selections.

The apparent permeability constants from the simulations were calculated according to Eq. (2).

$$P_{app} = \frac{r}{2c_w} \tag{2}$$

where $r$ is the number of water molecules crossing the membrane divided by the length of the simulations and the area of the lipid bilayer cross-section, and $c_w$ is the number of water molecules in the simulations divided by volume of the water [47]. The average volume of the water in the simulated buffer was determined by separately simulating a box containing 100 mM $CaCl_2$, 100 mM $MgCl_2$ in water only for 1.5 ns under identical simulation conditions.

In addition to permeability and saturation two more parameters were evaluated. First, the ordering of nonpolar hydrocarbon chains in the lipid bilayer characterized by the lipid order parameters, $S_{CH}$, given by Eq. (3).

$$S_{CH} = \frac{3}{2}\langle cos^2\theta \rangle - \frac{1}{2} \tag{3}$$

where θ is the angle between the CH bond (carbon-hydrogen bond) to the bilayer surface normal [48]. The angular brackets donate the time average. Second, density profiles were calculated using the VMD Density Profile Tool [49]. The program calculates a one-dimensional projection of selected atomic densities (atoms/Å3). The selected groups of molecules or atoms were water molecules within 3 Å of the lipid bilayer, phosphates in the lipid head groups and AMPs in systems with peptides present. The calculations were done with a 1 Å resolution and projected onto the z-axis of the system. For systems without AMPs present the $S_{CH}$ were calculated as an average for all lipids. In systems with AMPs present there were two selections. First, every lipid residue which had a contact point within 3 Å of a peptide. Second, the lipid residues which do not appear in the first selection. For systems without peptides, the average $S_{CH}$ of three parallel simulations were calculated and compared to the individual systems and parallel runs with peptides present. Both lipid order parameters and density profiles were calculated as an average over the last 195 ns of the simulation. Also, both parameters were calculated every 0.1 ns.

## Abbreviations

| | |
|---|---|
| NMR | Nuclear Magnetic Resonance |
| PVPA | Phospholipid Vesicle Permeability Assay |
| DMPC | 1,2-dimyristoyl-sn-glycero-3-phosphocholine |
| DMPG | 1,2-Dimyristoyl-sn-glycero-3-phospho-rac-(1-glycerol) |
| MOA | Mode of action |
| AMP | Antimicrobial Peptides |
| MIC | Minimal Inhibitory Concentration |

## CRediT authorship contribution statement

PR, MJ and JI designed and planned the project. PR and MJ established NMR procedures under the supervision of JI. MF prepared PVPA barriers under the supervision of GF. Modelling was done by RS under the supervision of JI and BOB. Figures were prepared by PR and RS. Original draft was written by PR, MJ, RS and JI. Funding for this project was acquired by JI. All authors interpreted data and commented on the final version of the manuscript.

## Declaration of competing interest

The authors declare that they have no known competing financial interests or personal relationships that could have appeared to influence the work reported in this paper.

## Acknowledgements

This project received funding from the DigiBiotics project of the Research Council of Norway (project ID 269425), the AntiBioSpec project of UiT the Arctic University of Norway (Cristin ID 20161326). The publication charges for this article have been funded by a grant from the publication fund of UiT the Arctic University of Norway. The simulations were performed on resources provided by UNINETT Sigma2 - the National Infrastructure for High Performance Computing and Data Storage in Norway, project nr. NN9888K.

## Appendix A. Supplementary data

Supplementary data to this article can be found online at https://doi.org/10.1016/j.bbamem.2022.183911.

## References


[1] O.collab <collab>World Health, Antimicrobial Resistance: Global Report on Surveillance, World Health Organization, Geneva, 2014.
[2] A.K. Marr, W.J. Gooderham, R.E. Hancock, Antibacterial peptides for therapeutic use: obstacles and realistic outlook, Curr. Opin. Pharmacol. 6 (5) (2006) 468–472.
[3] J.G. Hurdle, A.J. O'Neill, I. Chopra, R.E. Lee, Targeting bacterial membrane function: an underexploited mechanism for treating persistent infections, Nat. Rev. Microbiol. 9 (1) (2011) 62–75.
[4] J.D. Prajapati, U. Kleinekathöfer, M. Winterhalter, How to enter a bacterium: bacterial porins and the permeation of antibiotics, Chem. Rev. 121 (9) (2021) 5158–5192.
[5] M. Zasloff, Antimicrobial peptides of multicellular organisms, Nature 415 (6870) (2002) 389–395.
[6] J.M. Ageitos, A. Sánchez-Pérez, P. Calo-Mata, T.G. Villa, Antimicrobial peptides (AMPs): ancient compounds that represent novel weapons in the fight against bacteria, Biochem. Pharmacol. 133 (2017) 117–138.
[7] A. Hollmann, M. Martinez, P. Maturana, L.C. Semorile, P.C. Maffia, Antimicrobial peptides: interaction with model and biological membranes and synergism with chemical antibiotics, Front. Chem. 6 (2018) 204.
[8] W.C. Wimley, Describing the mechanism of antimicrobial peptide action with the interfacial activity model, ACS Chem. Biol. 5 (10) (2010) 905–917.
[9] E. Disalvo, Membrane Hydration: The Role of Water in the Structure and Function of Biological Membranes vol. 71, 2015.
[10] Q. Al-Awqati, One hundred years of membrane permeability: does Overton still rule? Nat. Cell Biol. 1 (8) (1999) E201–E202.
[11] S. Paula, A.G. Volkov, A.N. Van Hoek, T.H. Haines, D.W. Deamer, Permeation of protons, potassium ions, and small polar molecules through phospholipid bilayers as a function of membrane thickness, Biophys. J. 70 (1) (1996) 339–348.
[12] R. Kausik, S. Han, Dynamics and state of lipid bilayer-internal water unraveled with solution state 1H dynamic nuclear polarization, Phys. Chem. Chem. Phys. 13 (17) (2011) 7732–7746.
[13] D. Huster, A.J. Jin, K. Arnold, K. Gawrisch, Water permeability of polyunsaturated lipid membranes measured by 17O NMR, Biophys. J. 73 (2) (1997) 855–864.
[14] Y. Shai, Mode of action of membrane active antimicrobial peptides, Pept. Sci. 66 (4) (2002) 236–248.
[15] Y. Shai, Mechanism of membrane permeation and pore formation by antimicrobial peptides, in: Protein-Lipid Interactions, 2005, pp. 187–217.
[16] E. Gazit, I.R. Miller, P.C. Biggin, M.S. Sansom, Y. Shai, Structure and orientation of the mammalian antibacterial peptide cecropin P1 within phospholipid membranes, J. Mol. Biol. 258 (5) (1996) 860–870.
[17] J. Li, J.-J. Koh, S. Liu, R. Lakshminarayanan, C.S. Verma, R.W. Beuerman, Membrane active antimicrobial peptides: translating mechanistic insights to design, Front. Neurosci. 11 (73) (2017).
[18] G.E. Flaten, A.B. Dhanikula, K. Luthman, M. Brandl, Drug permeability across a phospholipid vesicle based barrier: a novel approach for studying passive diffusion, Eur. J. Pharm. Sci. 27 (1) (2006) 80–90.
[19] A. Engesland, M. Skar, T. Hansen, N. Škalko-basnet, G.E. Flaten, New applications of phospholipid vesicle-based permeation assay: permeation model mimicking skin barrier, J. Pharm. Sci. 102 (5) (2013) 1588–1600.
[20] M. Falavigna, M. Klitgaard, C. Brase, S. Ternullo, N. Škalko-Basnet, G.E. Flaten, Mucus-PVPA (mucus phospholipid vesicle-based permeation assay): an artificial permeability tool for drug screening and formulation development, Int. J. Pharm. 537 (1–2) (2018) 213–222.
[21] M. Falavigna, M. Pattacini, R. Wibel, F. Sonvico, N. Škalko-Basnet, G.E. Flaten, The vaginal-PVPA: a vaginal mucosa-mimicking in vitro permeation tool for evaluation of mucoadhesive formulations, Pharmaceutics 12 (6) (2020) 568.
[22] M. Falavigna, M. Klitgaard, E. Steene, G.E. Flaten, Mimicking regional and fasted/fed state conditions in the intestine with the mucus-PVPA in vitro model: the impact of pH and simulated intestinal fluids on drug permeability, Eur. J. Pharm. Sci. 132 (2019) 44–54.
[23] R. Rathinakumar, W.C. Wimley, High-throughput discovery of broad-spectrum peptide antibiotics, FASEB J. 24 (9) (2010) 3232–3238.
[24] A. Mónico, E. Martínez-Senra, F.J. Cañada, S. Zorrilla, D. Pérez-Sala, Drawbacks of dialysis procedures for removal of EDTA, PLOS ONE 12 (1) (2017), e0169843.
[25] B.E. Haug, W. Stensen, M. Kalaaji, Ø. Rekdal, J.S. Svendsen, Synthetic antimicrobial peptidomimetics with therapeutic potential, J. Med. Chem. 51 (14) (2008) 4306–4314.
[26] J. Svenson, W. Stensen, B.O. Brandsdal, B.E. Haug, J. Monrad, J.S. Svendsen, Antimicrobial peptides with stability toward tryptic degradation, Biochemistry 47 (12) (2008) 3777–3788.
[27] J. Håkansson, J.P. Cavanagh, W. Stensen, B. Mortensen, J.-S. Svendsen, J. Svenson, In vitro and in vivo antibacterial properties of peptide AMC-109 impregnated wound dressings and gels, J. Antibiot. 74 (5) (2021) 337–345.
[28] A.D.C. França, T.P. Sudbrack, N.L. Archilha, R. Itri, K.A. Riske, Effects caused by triton X-100 on lipid bilayers of different composition, Biophys. J. 102 (2012).
[29] J. Isaksson, B.O. Brandsdal, M. Engqvist, G.E. Flaten, J.S.M. Svendsen, W. Stensen, A synthetic antimicrobial peptidomimetic (LTX 109): stereochemical impact on membrane disruption, J. Med. Chem. 54 (16) (2011) 5786–5795.
[30] A. Slezak, B. Turczynski, Modification of the Kedem-Katchalsky equations, Biophys. Chem. 24 (2) (1986) 173–178.
[31] O. Kedem, A. Katchalsky, Thermodynamic analysis of the permeability of biological membranes to non-electrolytes, Biochim. Biophys. Acta 27 (1958) 229–246.
[32] R. Koynova, M. Caffrey, Phases and phase transitions of the phosphatidylcholines, Biochim. Biophys. Acta Rev. Biomembr. 1376 (1) (1998) 91–145.
[33] M.M.A.E. Claessens, B.F. van Oort, F.A.M. Leermakers, F.A. Hoekstra, M.A. Cohen Stuart, Charged lipid vesicles: effects of salts on bending rigidity, stability, and size, Biophys. J. 87 (6) (2004) 3882–3893.
[34] H.-T. Chou, H.-W. Wen, T.-Y. Kuo, C.-C. Lin, W.-J. Chen, Interaction of cationic antimicrobial peptides with phospholipid vesicles and their antibacterial activity, Peptides 31 (10) (2010) 1811–1820.
[35] M.-A. Sani, F. Separovic, How membrane-active peptides get into lipid membranes, Acc. Chem. Res. 49 (6) (2016) 1130–1138.
[36] J.C. Mathai, S. Tristram-Nagle, J.F. Nagle, M.L. Zeidel, Structural determinants of water permeability through the lipid membrane, J. Gen. Physiol. 131 (1) (2008) 69–76.
[37] B. Maherani, E. Arab-Tehrany, A. Kheirolomoom, D. Geny, M. Linder, Calcein release behavior from liposomal bilayer; influence of physicochemical/mechanical/structural properties of lipids, Biochimie 95 (11) (2013) 2018–2033.
[38] K. Vanommeslaeghe, E. Hatcher, C. Acharya, S. Kundu, S. Zhong, J. Shim, E. Darian, O. Guvench, P. Lopes, I. Vorobyov, A.D. Mackerell Jr., CHARMM general force field: A force field for drug-like molecules compatible with the CHARMM all-atom additive biological force fields, J. Comput. Chem. 31 (4) (2010) 671–690.
[39] R.B. Best, X. Zhu, J. Shim, P.E.M. Lopes, J. Mittal, M. Feig, A.D. MacKerell, Optimization of the additive CHARMM all-atom protein force field targeting improved sampling of the backbone ϕ, ψ and side-chain χ1 and χ2 dihedral angles, J. Chem. Theory Comput. 8 (9) (2012) 3257–3273.
[40] S. Jo, J.B. Lim, J.B. Klauda, W. Im, CHARMM-GUI membrane builder for mixed bilayers and its application to yeast membranes, Biophys. J. 97 (1) (2009) 50–58.
[41] W. Humphrey, A. Dalke, K. Schulten, VMD: visual molecular dynamics, J. Mol. Graph. 14 (1) (1996), 33-8, 27-8.
[42] J.C. Phillips, R. Braun, W. Wang, J. Gumbart, E. Tajkhorshid, E. Villa, C. Chipot, R. D. Skeel, L. Kalé, K. Schulten, Scalable molecular dynamics with NAMD, J. Comput. Chem. 26 (16) (2005) 1781–1802.
[43] J.B. Klauda, R.M. Venable, J.A. Freites, J.W. O'Connor, D.J. Tobias, C. Mondragon-Ramirez, I. Vorobyov, A.D. MacKerell, R.W. Pastor, Update of the CHARMM all-atom additive force field for lipids: validation on six lipid types, J. Phys. Chem. B 114 (23) (2010) 7830–7843.
[44] S.E. Feller, Y. Zhang, R.W. Pastor, B.R. Brooks, Constant pressure molecular dynamics simulation: the Langevin piston method, J. Chem. Phys. 103 (11) (1995) 4613–4621.
[45] U. Essmann, L. Perera, M.L. Berkowitz, T. Darden, H. Lee, L.G. Pedersen, A smooth particle mesh Ewald method, J. Chem. Phys. 103 (19) (1995) 8577–8593.
[46] J.-P. Ryckaert, G. Ciccotti, H.J.C. Berendsen, Numerical integration of the cartesian equations of motion of a system with constraints: molecular dynamics of n-alkanes, J. Comput. Phys. 23 (3) (1977) 327–341.
[47] R.M. Venable, A. Krämer, R.W. Pastor, Molecular dynamics simulations of membrane permeability, Chem. Rev. 119 (9) (2019) 5954–5997.
[48] L.S. Vermeer, B.L. de Groot, V. Réat, A. Milon, J. Czaplicki, Acyl chain order parameter profiles in phospholipid bilayers: computation from molecular dynamics simulations and comparison with 2H NMR experiments, Eur. Biophys. J. 36 (8) (2007) 919–931.
[49] T. Giorgino, Computing 1-D atomic densities in macromolecular simulations: the density profile tool for VMD, Comput. Phys. Commun. 185 (1) (2014) 317–322.